TOXICOLOGICAL SCIENCES **110(1)**, 138–155 (2009)
doi:10.1093/toxsci/kfp087
Advance Access publication May 4, 2009

Mechanisms of Quantum Dot Nanoparticle Cellular Uptake

Leshuai W. Zhang and Nancy A. Monteiro-Riviere[1]

Center for Chemical Toxicology Research and Pharmacokinetics, Department of Clinical Science, North Carolina State University, Raleigh, North Carolina 27606

Received March 6, 2009; accepted April 22, 2009

Due to the superior photoemission and photostability characteristics, quantum dots (QD) are novel tools in biological and medical applications. However, the toxicity and mechanism of QD uptake are poorly understood. QD nanoparticles with an emission wavelength of 655 nm are ellipsoid in shape and consist of a cadmium/selenide core with a zinc sulfide shell. We have shown that QD with a carboxylic acid surface coating were recognized by lipid rafts but not by clathrin or caveolae in human epidermal keratinocytes (HEKs). QD were internalized into early endosomes and then transferred to late endosomes or lysosomes. In addition, 24 endocytic interfering agents were used to investigate the mechanism by which QD enter cells. Our results showed that QD endocytic pathways are primarily regulated by the G-protein–coupled receptor associated pathway and low density lipoprotein receptor/scavenger receptor, whereas other endocytic interfering agents may play a role but with less of an inhibitory effect. Lastly, low toxicity of QD was shown with the 20nM dose in HEK at 48 h but not at 24 h by the live/dead cell assay. QD induced more actin filaments formation in the cytoplasm, which is different from the actin depolymerization by cadmium. These findings provide insight into the specific mechanism of QD nanoparticle uptake in cells. The surface coating, size, and charge of QD nanoparticles are important parameters in determining how nanoparticle uptake occurs in mammalian cells for cancer diagnosis and treatment, and drug delivery.

Key Words: **quantum dot nanoparticles; endocytosis; lipid rafts; G-protein–coupled receptor; scavenger receptor; cytotoxicity.**

The explosive growth in the nanotechnology industry leads to a large number of novel nanomaterials for biomedical applications, yet the knowledge regarding their toxicity is minimal. Many nanomaterials have been shown to become localized within cells. Coated magnetite nanoparticles (NPs) were found in human mammary carcinoma cells (Jordan *et al*., 1999; Zhang *et al*., 2002). Poly(D,L-lactide-*co*-glycolide) NP-containing 6-coumarin as a fluorescent marker were internalized in cultured rabbit conjunctival epithelial cells (Qaddoumi *et al*., 2004). Functionalized fullerenes have been localized in human fibroblasts (Sayes *et al*., 2004) and human epidermal keratinocytes (HEKs) (Rouse *et al*., 2006). Both multiwalled carbon nanotubes (Monteiro-Riviere *et al*., 2005) and functionalized single-walled carbon nanotubes have been localized in the cytoplasmic vacuoles of HEK (Zhang *et al*., 2007). Quantum dot (QD) nanoparticles are of special interest because they have been used as fluorescent probes for biomedical applications, especially cellular imaging. Many dyes and contrast agents are unstable and therefore the QD physicochemical parameters including chemical composition, surface charge, small size, water solubility, and fluorescence stability enable QD to be utilized as ideal agents for intracellular tracking or biomedical imaging or as a model for drug delivery of active molecules and diagnostics.

QD are bright photostable semiconductor heterogeneous nanocrystals that consist of a colloidal core surrounded by one or more surface coatings. Shell coatings are frequently applied in one or more layers to increase solubility in aqueous medium, reduce leaching of metals from the core, and facilitate customized surface chemistries for the attachment of conjugates to therapeutic and diagnostic macromolecules, receptor ligands, or antibodies (Derfus *et al*., 2004; Michalet *et al*., 2005). Unlike other engineered nanostructures, QD are easily detected due to an unusually intense and photostable fluorescence and are commercially available in various sizes and shapes with diverse surface coatings, making QD useful tools to determine the cellular uptake pathways of small particles. These unique fluorescence properties with specific surface functionalizations have been used in cell imaging, immunohistochemistry, and cancer targeting (Gao *et al*., 2004; Xing *et al*., 2007). Negatively charged QD coated with dihydrolipoic acid or positively charged QD coated with polyethylene glycol (PEG) attached with a polyethylenimine coating can be incorporated into human cells (Duan and Nie, 2007; Jaiswal *et al*., 2003). Our laboratory showed QD with a CdSe core and CdS (Zhang *et al*., 2008) or ZnS shell (Ryman-Rasmussen *et al*., 2007a, b), were capable of entering HEK. A series of carboxylic acid–coated QD with different emission wavelengths are now available commercially to track proteins in cells (Invitrogen website, 2009). These QD consist

[1] To whom correspondence should be addressed at Center for Chemical Toxicology Research and Pharmacokinetics, Department of Clinical Science, North Carolina State University, 4700 Hillsborough Street, Raleigh, NC 27606. Fax: (919) 513-6358. E-mail: Nancy_Monteiro@ncsu.edu.

of a CdSe core/ZnS shell and can be coated with PEG, PEG-amine (NH_2), or carboxylic acid (COOH). However, the mechanism of cellular uptake is unknown and the toxicity of nanoparticles within biological systems is a concern.

NP uptake by cells may occur through several different mechanisms, and classified into phagocytosis and pinocytosis. Pinocytosis includes macropinocytosis with uptake of particles > 1 μm, clathrin or caveolae-mediated endocytosis, or clathrin/caveolae independent endocytosis. Caveolae consist of plasma membrane invaginations of 50- to 80-nm size containing cholesterol and sphingolipids, receptors and caveolins (Lajoie and Nabi, 2007; Pelkmans *et al*., 2002). Endocytosis of various membrane receptors may also occur via lipid rafts (Nichols, 2003). Lipid rafts provide a platform for the assembly of receptors, adaptors, regulators, and other downstream proteins as a signaling complex, and may be joined with caveolae. Clathrin-coated pits of 100–200 nm have been shown to be associated with the key protein clathrin and other scaffold proteins such as AP-2 and eps15 (Ehrlich *et al*., 2004). Macropinocytosis is a form of endocytosis related to cell surface ruffling and provides a route for non-selective endocytosis of solute macromolecules. Macropinosomes are more than 0.2 μm in diameter, and may be as large as 5 μm (Swanson and Watts, 1995). Specialized phagocytosis via protease activation receptor 2 occurs in HEK that take up melanosomes from adjacent melanocytes. It is possible that NP may be taken up by cells via their size selectivity that may match those of endocytic pits.

NP endocytosis by cells not only depends on the size of the NP, but also the surface coating and charge. Carboxydextran-coated superparamagnetic iron oxide nanoparticles (SPION) were internalized by human mesenchymal stem cells, and the efficiency of uptake was correlated to the amount of carboxyl groups on the NP surface (Mailander *et al*., 2008). Cationic D,L-polylactide (PLA)-NP entered Hela cells in greater amounts than anionic PLA-NP (Dausend *et al*., 2008; Harush-Frenkel *et al*., 2007). NP uptake may also depend on the length of the surface coating (Chang *et al*., 2006), or the type of cells (Xia *et al*., 2008). However, the specific endocytic mechanism by which cells internalize specific NP such as QD remains unknown but the mechanism of cellular uptake is important in the field of nanomedicine, cancer diagnosis, and treatment.

In this study, we evaluated 24 potential endocytic inhibitors that may be classified into seven major groups based on their effects in cells (Table 1): cytoskeleton, caveolae/lipid rafts, clathrin, macropinocytosis, G-protein coupled receptor (GPCR)-associated pathway, melanosome transfer mediated pathway, and low density lipoprotein/scavenger receptor related pathway. The effects of these inhibitors on QD uptake were evaluated by flow cytometry for inhibition quantification and also viewed by confocal laser scanning microscopy (CLSM) for fluorescence imaging. We also investigated whether QD endocytosis was receptor-mediated. Furthermore, the localization of QD on the cell membrane or in the cytoplasm was examined with organelle markers. Lastly, because QD aggregates remain in lysosomes, the potential toxicity in the acidic compartment was evaluated by viability and F-actin cytoskeleton methods. These findings provide information on the specific endocytic pathway that QD NP utilize and help understand the mechanism of penetration into cells that could be used for diagnosis and treatment of cancer.

TABLE 1
Inhibitors and their Function and Concentration

Name	Function	Final conc.
Nocodazole	Disrupts microtubule (cytoskeleton)	10.0 μg/ml
CytD	Inhibit F-actin polymerization (cytoskeleton)	10.0 μg/ml
MβCD	Cholesterol-depletion reagent (caveolae/ lipid rafts)	5.0 mg/ml
Lovastatin	Cholesterol depletion (caveolae/lipid rafts)	10.0 μg/ml
Genistein	Inhibit F-actin recruitment to clathrin pits [a] (clathrin)	10.0 μg/ml
CPM	Inhibitor of Rho GTPase (clathrin)	10.0 μg/ml
Y-27632	Related to cytoskeleton and melanosome transfer [b]	10.0 μg/ml
NaN_3	ATP inhibitor (ATP)	3.0 mg/ml
DMA	Na^+/H^+ exchanger inhibitor (macropinocytosis)	10.0 μg/ml
WMN	PI3K inhibitor (macropinocytosis)	100.0 ng/ml
LY	PI3K inhibitor (macropinocytosis)	10.0 μg/ml
PTX	Inhibitor of G_i α subunit (GPCR)	100.0 ng/ml
CTX	Activator of G_s α subunit (GPCR)	1.0 μg/ml
U-73122	PLC inhibitor (down stream of GPCR)	4.0 μg/ml
SRP	PKC inhibitor (down stream of GPCR)	1.0 μg/ml
TrpI	Inhibitor of PAR-2 pathway (melanosome)	1.0 mg/ml
NCM	Melanosome inhibition (melanosome)	122.1 μg/ml
BMA1	Inhibits endosome acidification (endosome)	100.0 ng/ml
CRQ	Inhibits endosome acidification (endosome)	125.0 μg/ml
BFA	Interferes with Golgi, endosome and lysososome	10.0 μg/ml
PolyI	Scavenger receptor inhibitor	10.0 μg/ml
FCD	Scavenger receptor inhibitor	10.0 μg/ml
LDL	Ligands for LDL receptor	10.0 μg/ml
AcLDL	Ligands for scavenger receptor	10.0 μg/ml

Note. a = Genistein inhibits tyrosine kinase activities that can phosphorylate actin and recruit the cytoskeleton proteins to clathrin-coated pits and enhance the internalization of clathrin mediated endocytosis. b = Y-27632 is the inhibitor of ROCK and abolishes actin filaments. It is also used to inhibit melanosome transfer to keratinocytes via protease-activated receptor 2 (PAR-2) pathway.

MATERIALS AND METHODS

Quantum dots. QD with a CdSe core and ZnS shell were obtained from Molecular Probe/Invitrogen (Eugene, OR). QD with emission maxima at 655 nm (QD655) have an ellipsoid core/shell with diameters of 6 nm (minor axis) by 12 nm (major axis). Each size was obtained with three different surface coatings: PEG, PEG-amine, or polyacrylic acid (carboxylic acids, COOH). These coatings are, respectively, neutral, positive, or negatively charged as supplied at physiological pH. The hydrodynamic diameters were measured by

size exclusion chromatography on high-performance liquid chromatography with a major axis for QD655 were 45 nm (PEG), 20 nm (PEG-amine), and 18 nm (COOH). QD were sold as Qtrackers Nontargeted Quantum Dots (PEG) or Qdots ITK Amino (PEG) or Carboxyl QD, respectively. QD were supplied at concentrations ranging from 2 to 8.7mM in a 50mM borate buffer of pH 9.0 (carboxylic acid–coated QD) or pH 8.3 (PEG and PEG-amine–coated QD) (Ryman-Rasmussen *et al*., 2006). The size distribution is estimated at 3% based on TEM. Typically, it is estimated that there are 800–1200 carboxylic acid per QD (Molecular Probe/Invitrogen). The polydispersity index measurement is not particularly useful for an engineered construct such as this due to the large dissimilarity between the molecular weights of the constituents (e.g., cadmium vs. carbon) and not provided by the manufacturer.

Reagents and antibodies. Mouse antibodies for human caveolin 1, clathrin (heavy chain), EEA1, lysosome-associated membrane glycoproteins 1 (LAMP1) (CD107a), CD63, were purchased from BD Biosciences (San Jose, CA). Live/dead cell assay, normal goat serum, BODIPY FL phallacidin, Alexa fluor 488 conjugated cholera toxin B (CTB), Alexa fluor 488 F(ab')$_2$ fragment of goat anti-mouse IgG, LDL, AcLDL were purchased from Molecular Probes, Invitrogen (Eugene, OR). All the inhibitors, including nocodazole, cytochalasin D (CytD), methyl-β-cyclodextrin (MβCD), lovastatin, U-73122, Y-27632, genistein, 5-(N,N-dimethyl)-amiloride (DMA), sodium azide (NaN_3), wortmannin (WMN), Ly294002 (LY), pertussis toxin (PTX), cholera toxin (CTX), staurosporine (SRP), bafilomycin A1 (BMA1), chloroquine (CRQ), trypsin inhibitor (TrpI), niacinamide (NCM), chlorpromazine (CPM), brefeldin A (BFA), polyI, and fuicodan (FCD), are from Sigma-Aldrich (St Louis, MO).

Transmission electron microscopy. To determine the morphology of QD655-COOH in water or in media of the cells, QD (20nM) were incubated at 37°C for 24 h in water or prepared in keratinocyte growth medium 2 (KGM-2) with borate buffer for stability. Solutions were diluted in water, and 10 μl of the solution was placed on formvar-coated grids for transmission electron microscopy (TEM). To observe QD localization in cells, HEK were treated with 20nM of QD for 24 h, rinsed, and fixed in Trump's fixative and routinely processed for TEM and viewed on a Philips EM208S transmission electron microscope.

Fluorescence quantification of QD using a spectrofluorometer. To quantitate the uptake dynamics of QD by a spectrofluorometer, neonatal HEK (Cambrex, Corp, Walkersville, MD) were seeded in 24-well plates, and then incubated with 2nM of QD for 2, 6, 12, and 24 h. Note that 250,000 cells per well occupied around 90% the area of each well to exclude QD non-specific binding on the plastic bottom of the well, and Millex syringe driven filter with 0.22-μm pore (Milipore Corporation, Bedford, MA) was used to filter QD in KGM-2 to remove the large aggregates of QD in KGM-2. The cells were then washed by Hanks' balanced salt solution (HBSS) and assayed on a tunable Gemini EM microplate spectrofluorometer (Molecular Devices, Downingtown, PA). The excitation wavelength was 360 nm and the emission wavelength at 655 nm with a cut off of 610 nm. Controls consisted of background fluorescence without QD.

Chemical and immunostaining. To observe the colocalization of CTB and QD, CTB (Alexa Fluor 488 labeling) was incubated with HEK along with QD, fixed as above and observed by CLSM. For all other staining, cells were washed and fixed. Cells were permeabilized by 0.1% Triton X-100, blocked with 5% normal goat serum. Cells were washed and F-actin stained by BODIPY FL phallacidin for 20 min, or mouse anti-human antibodies at 5 μg/ml for 1 h and were incubated with Alexa fluor 488 F(ab')$_2$ fragment of goat anti-mouse IgG at 5 μg/ml for 1 h. Live/dead assay (Invitrogen Corp.) was performed on HEK in 24 wells dosed with 20nM of QD for 24 h. HEK were washed, stained with ethidium homodimer-1(EthD-1; 2μM) and calcein AM (CAM; 1μM), fixed, embedded for CLSM.

CLSM and fluorescence microscopy. All samples were analyzed by a Leica TCS SP1 confocal laser scanner interfaced to an inverted Leica IMBE microscope with an X40 plan apochromat objective. The microscope was equipped with a confocal differential interference contrast (DIC) system. QD were excited with a UV (351 and 364 nm) and an argon laser (488 nm) with emission channels of 645–665 nm for QD. Alexa fluor 488 conjugates, calcein AM (CAM), or fluorescein isothiocyanate (FITC)-labeled fluorochrome were excited with argon laser (488 nm) with emission channels of 510–540 nm. Alexa Fluor 546 conjugates were excited by krypton-argon laser (568 nm) with emission channels of 572–600 nm. Ethidium homodimer-1 (EthD-1) was exited by krypton-argon laser and the emission channels of 590–610 nm were collected. Z-series optical sections were taken at 0.3-μm intervals, and three-dimensional images were captured and assembled by using LCS Lite software and showed as Supplementary video 1. In CLSM, the autofluorescence does not appear in cultured human epidermal keratinocytes especially when excited by the UV light or argon laser and collected at ~655 nm. Samples were also analyzed on a Olympus X71 fluorescence microscope (Olympus, Tokyo, Japan).

Sample preparation for flow cytometry. HEK were seeded in 24-well plates and dosed with QD with/without inhibitors. Table 1 describes the inhibitors used and their function/concentration. Cells were washed in HBSS, suspended and neutralized by trypsin-ethylenediaminetetraacetic acid, centrifuged and resuspended, fixed and analyzed in BD FACScan Flow Cytometer (BD Science, San Jose, CA) with 10,000 cells gated on the basis of forward and side scatter. A 488-nm laser was used to excite the QD and the data stored and processed using CellQuest Pro software (San Jose, CA).

Quantification for QD uptake inhibitory effects by inhibitors. Cells that were incubated with QD with/without inhibitors were washed, suspended and fixed for flow cytometry. The inhibition effects were calculated using the following formula and the results listed in Supplementary Table 2: inhibitory effects = (mean fluorescence intensity for inhibitor sample X% of gated HEK - mean fluorescence intensity for cell only sample X% of gated HEK)/(mean fluorescence intensity for control sample X% of gated HEK - mean fluorescence intensity for cell only sample X% of gated HEK). The gated line separates the HEK with high fluorescent intensities from the cells in the negative control that were not treated with QD.

Size and zeta-potential determination. QD655-COOH was diluted by 100mM phosphate buffer (PBS) at the pH of 4.5, 5, 5.5, 6, 7, 8, 9. Size and zeta-potential of QD were examined by Zeta-sizer Nano-ZS (Malvern Instruments Inc., Worcestershire, UK) with a 633-nm laser. To exclude any extraneous signals in the scattered light intensity due to sample fluorescence, a narrow band filter with a wavelength centered at 632.8 nm with a bandwidth of 10 nm was used.

Statistical analysis. The mean values of inhibition effects (normalized to control) with different inhibitors with a series of concentration were calculated and the significant differences ($p < 0.05$) determined using PROC GLM Procedure (SAS 9.1 for Windows; SAS Institute, Cary, NC). When significant differences were found, multiple comparisons were performed using Tukey's studentized range HSD test at $p < 0.05$ level of significance.

RESULTS

QD Uptake is Determined by Surface Coatings

Figure 1 shows that only a few HEK internalized PEG (Fig. 1C) or PEG-amine (Fig. 1D) coated QD at 20nM, whereas carboxylic coated (QD655-COOH) at 2nM were taken up in greater amounts and localized around the periphery of the nuclei at 24 h (Fig. 1A) but more agglomeration was noted with the 20nM of QD655-COOH (Fig. 1B). Therefore, we depicted a series of experiments to investigate the endocytic mechanisms only with QD655-COOH due to the high efficiency uptake with the carboxylic acid coating. TEM was used to visualize the QD655-COOH (Referred as "QD"

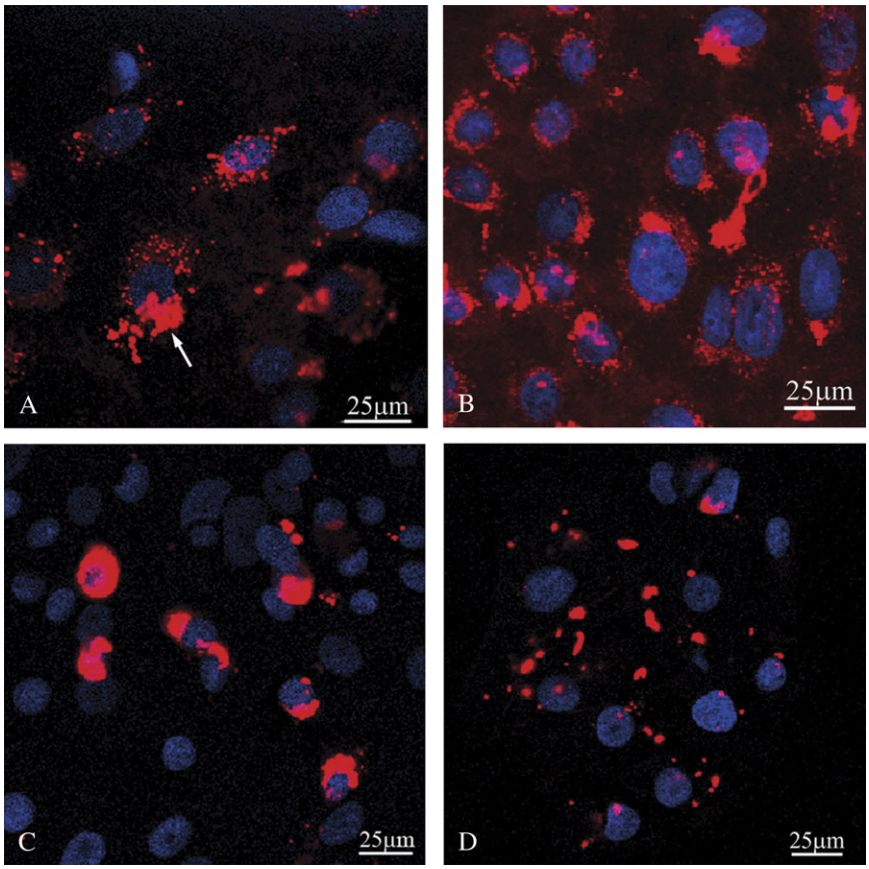

FIG. 1. QD655 with different coatings in HEK. QD coated with carboxylic acid (COOH), PEG, PEG-amine (NH_2) were incubated with HEK for 24 h. (A) QD655-COOH at 2nM, note the punctate areas at the peripheral of the nucleus. The large agglomerates are indicated by an arrow. Z-stack analysis by CLSM determined that the agglomerates were mainly on the surface of the cells. (B) QD655-COOH at 20nM shows clear large QD agglomerates at both poles of the nuclei. (C) QD655-PEG at 20nM. The horseshoe pattern that fills most of the cytoplasm is evident. (D) QD655-NH_2 at 20nM did not show QD in the cytoplasm except some agglomerates (smaller than those of PGE-coated QD) were found on the surface of cells and determined by DIC and by Z-stack analysis.

until specified) subcellular localization in HEK at 24 h. At 20nM, QD were found primarily around the periphery of the nuclear membrane and in intracytoplasmic vacuoles (Fig. 2A). The elliptical shape of the individual QD can be visualized at higher magnification (Fig. 2B). QD in water appeared normal, whereas QD in KGM-2 tend to stick along the edge of the precipitated proteins at 24 h (Fig. 2C). In addition, QD did not change in shape based on TEM when incubated with serum free KGM-2 suggesting QD are stable in the cell culture medium (Fig. 2C). Live CLSM was utilized to observe the QD uptake until 8 h (data not shown). At 30 min, QD were distributed throughout the entire cytoplasm, showing localization in the subcellular compartments and forming punctate areas with weak fluorescence. Later, the punctate fluorescence areas increased in intensity and gradually formed around the periphery of the nuclei. Three-dimensional images of QD internalization at 30 min are shown as Supplementary Video 1. The fluorescence intensity of QD associated with cells increased with time and became saturated at 12 h quantitated by a spectrofluorometer. These studies suggest the physicochemical parameters of QD may affect nanoparticle uptake in cells, the precise mechanism of QD endocytosis and internalization into the subcellular organelles may require receptor recognition which is the focused of the study.

QD were Recognized by Lipid Rafts

To investigate if QD uptake is mediated by clathrin or caveolae, QD were incubated with HEK and stained with clathrin and caveolin 1. Our study showed that caveolin 1, a marker for caveolae, had slight colocalization with QD at 1 h, whereas clathrin and the adaptor protein eps15 of clathrin did not colocalize with QD at 1 h (Fig. 3A). In addition, QD were coincubated with cholera toxin B (CTB, conjugated with Alexa Fluor 488), a lipid raft marker. CTB colocalized with QD at 15 min (Fig. 3B), but colocalization decreased and showed greater fluorescence with a punctate pattern at 30 min (Supplementary Fig. 1) and 1 h (Fig. 3B). In addition, CTB and QD competed with each other so that cells containing large amounts of QD were not stained by CTB (Supplementary Fig. 1), suggesting CTB and QD may occupy some of the same lipid raft sites on the cell membrane.

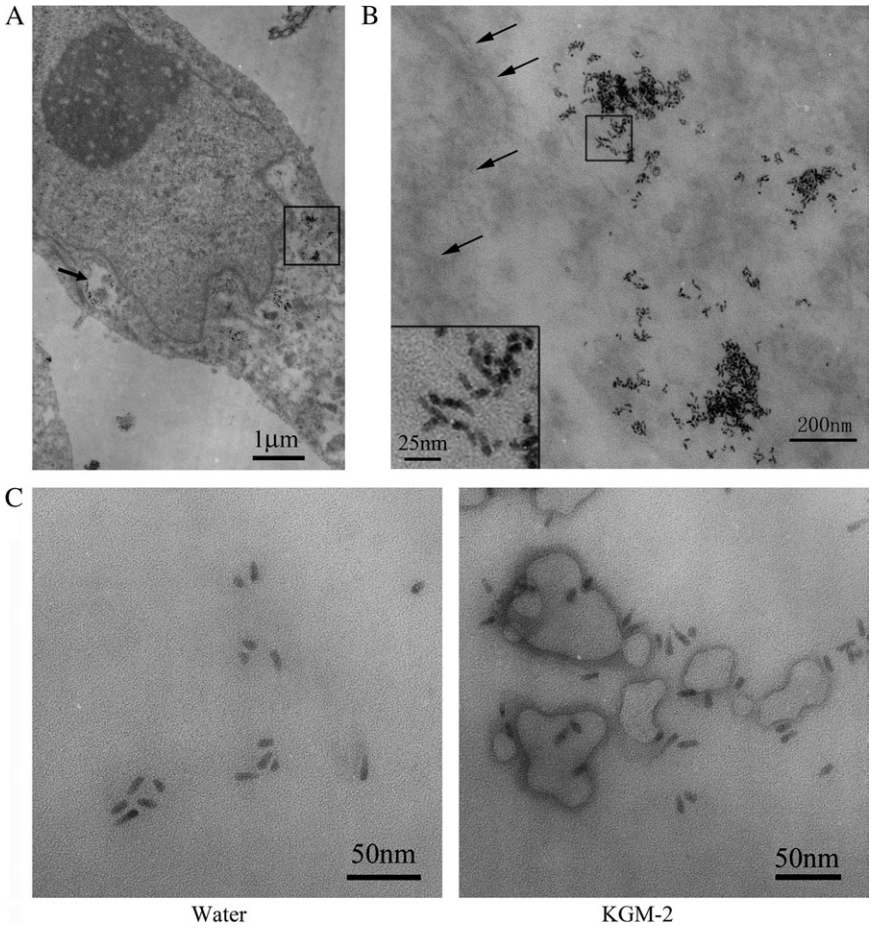

FIG. 2. TEM of QD655-COOH in HEK for 24 h. (A) HEK depicting the localization of QD655-COOH (20nM) at the periphery of the nuclear membrane (insert) and in cytoplasmic vacuoles (arrow). (B) Higher magnification of the insert in (A) showing individual QD (bottom left) and along the nuclear membrane (arrow). (C) QDs were incubated in water or serum-free KGM-2 at 37°C for 24 h.

To further support the hypothesis that QD endocytosis is via the lipid raft/caveolae pathway but not the clathrin dependent pathway, cholesterol-depletion reagents such as methyl-β-cyclodextrin (MβCD) and lovastatin, or clathrin endocytic inhibitor CPM, were used. If QD fluorescence stability was affected by some of the endocytic interfering agents (inhibitors), the cells were first pre-treated with the inhibitors for 1 h, then treated with QD for 30 min (preincubation method). If QD fluorescence stability was not affected by the inhibitors, then the pretreated cells can be treated with QD and the inhibitors together for 30 min to confirm if there was a continuous inhibitory effect on the cells, and will be referred to as the coincubation method. All cells were washed, suspended and fixed for CLSM or FCM. The Supplementary Table 1 describes the stability of QD influenced by the inhibitors in greater detail. QD uptake inhibitory effects with all different inhibitors were evaluated by FCM and the results showed in Supplementary Table 2. Inhibitory effects of MβCD and lovastatin were seen by CLSM (Fig. 3C); uptake of QD was reduced to 52.9% by MβCD coincubation in a concentration-dependent manner (Fig. 3D). In comparison, CPM did not inhibit QD uptake (Supplementary Table 2). Therefore, lipid rafts may provide a platform for the assembly of QD, receptors, adaptors, and regulators as a signaling complex and may be joined with caveolae/lipid raft but not clathrin.

QD Translocation into Endosomes

Internalized macromolecules are normally translocated via endosome and lysosomes containing varying amounts of hydrolases which often leads to rapid destruction and degradation of macromolecules (Tjelle *et al.*, 1996). After QD were internalized into the cytoplasm of HEK, early endosomes were formed via membrane invagination that engulfed the QD, which was demonstrated by their colocalization with an early endosome marker, EEA1 at 1 h; colocalization gradually decreased with time and was not present at 12 h (Fig. 4A). The early endosome acidification slowly formed late endosome and lysosome that was recognized by CD63 and LAMP1, respectively. QD did not colocalize with CD63 at 1 h, whereas colocalization was found

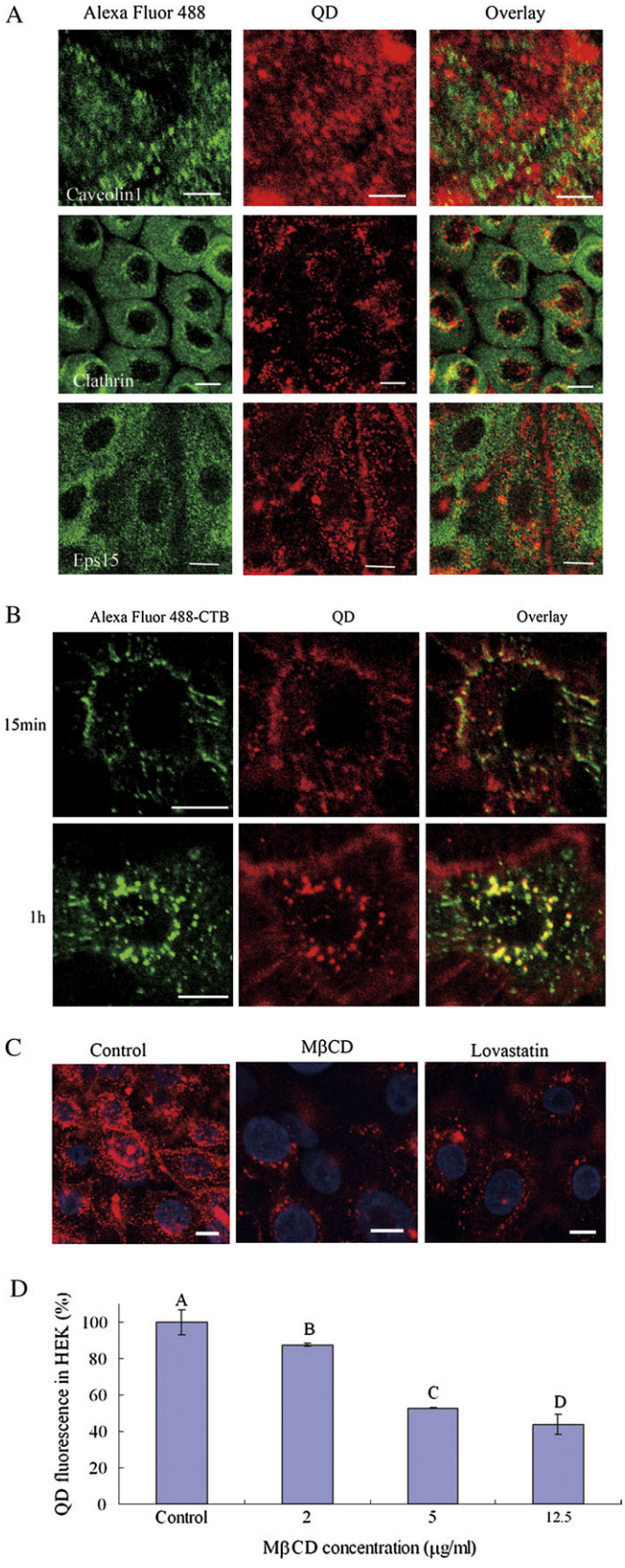

FIG. 3. QD colocalization with caveolin 1, clathrin, eps15, or a lipid raft marker. (A) HEKs were incubated with QD for 1 h and caveolin 1, clathrin, and eps15 were stained. Top row, caveolin 1 staining and its minor colocalization with QD. Middle row, clathrin staining depicting no colocalization with QD at 1 h. Bottom row, the clathrin adaptor protein, eps15 staining did not localize with QD at 1 h. Scale bar = 10 μm. (B) QD colocalization with lipid raft (stained by Alexa Fluor 488 conjugated CTB) at 15 min and 1 h. Left column, CTB-Alexa 488 staining (green); middle column, QD (red); right column, overlay of CTB and QD (yellow). Scale bar = 10 μm. (C) QD uptake inhibition by MβCD or Lovastatin at 30 min. Nuclei are labeled with DAPI (blue). Scale bar = 10 μm. (D) QD uptake inhibitory effects by MβCD are dose dependent. The QD fluorescence associated with cells was quantified by FCM. The inhibition effects are shown as the fluorescence (percentage) relative to controls. Mean ± SE are the average of duplicates ($p < 0.05$, Tukey HSD test). Histogram with different letters (A, B, C, and D) denote mean values that are statistically different at $p < 0.05$.

at 6 h (data not shown) and 12 h, and the strongest colocalization occurred at 24 h (Fig. 4B). Similar increase in QD colocalizations with LAMP1 was noted from 6 h to 24 h (Supplementary Fig. 2). This suggests that QD were localized within late endosomes or lysosomes. To further support this hypothesis, endosome interfering reagents bafilomycin A1 (BMA1), chloroquine (CRQ), and brefeldin A (BFA) were used. BMA1 and CRQ can inhibit endosome acidification and thereby could serve as potential inhibitors of QD uptake and their subsequent fusion during late endosome formation (Seglen, 1983; van Weert *et al.*, 1995). BMA1 and CRQ slightly reduced QD uptake observed with CLSM when coincubated with QD (Fig. 5A). The inhibitory effect of CRQ on QD endocytosis was dose dependent when evaluated by FCM (Fig. 5B). The slight inhibitory effect did not occur with preincubation, suggesting their role in post-uptake inhibition. Furthermore, the failure of colocalization of QD and CD63 by BMA1 or CRQ at 6 h prevented the uptake of QD in the late endosome (Supplementary Fig. 3). BFA interfered with endosome formation by inducing tubulation of the Golgi complex, endosome and lysosome membrane (Wagner *et al.*, 1994). QD uptake was inhibited by BFA as evaluated by FCM, and QD distribution presented tubulated-liked pattern suggesting QD in endosome tracking with trans-Golgi tubular network (Fig. 5A). BFA at 1.6, 4, and 10 μg/ml were able to attenuate QD uptake to the same extent by FCM (79.1% for 1.6 μg/ml and 77.24% for 10 μg/ml compared with control). The phenomenon that preincubation and coincubation of BFA led to similar inhibitory effects (Supplementary Table 2) illustrate that QD uptake inhibition by subcellular organelles is sensitive and consistent. The pH value in the endocytic compartments decreases from early endosomes (5.9–6.0) to lysosomes (5.0–5.5) in Chinese hamster ovary cells (Mukherjee *et al.*, 1997). The pH in lysosomes can be as low as 4.5 (Asokan and Cho, 2002). We showed that QD were not stable in PBS at pH 4.5–5 when evaluated by dynamic light scattering (DLS) (Fig. 5C), suggesting the possible aggregation of QD in late endosomes and lysosomes. Moreover, the zeta-potential at pH 4.5 was −18 mV (Fig. 5D) (< −30 mV, stable),

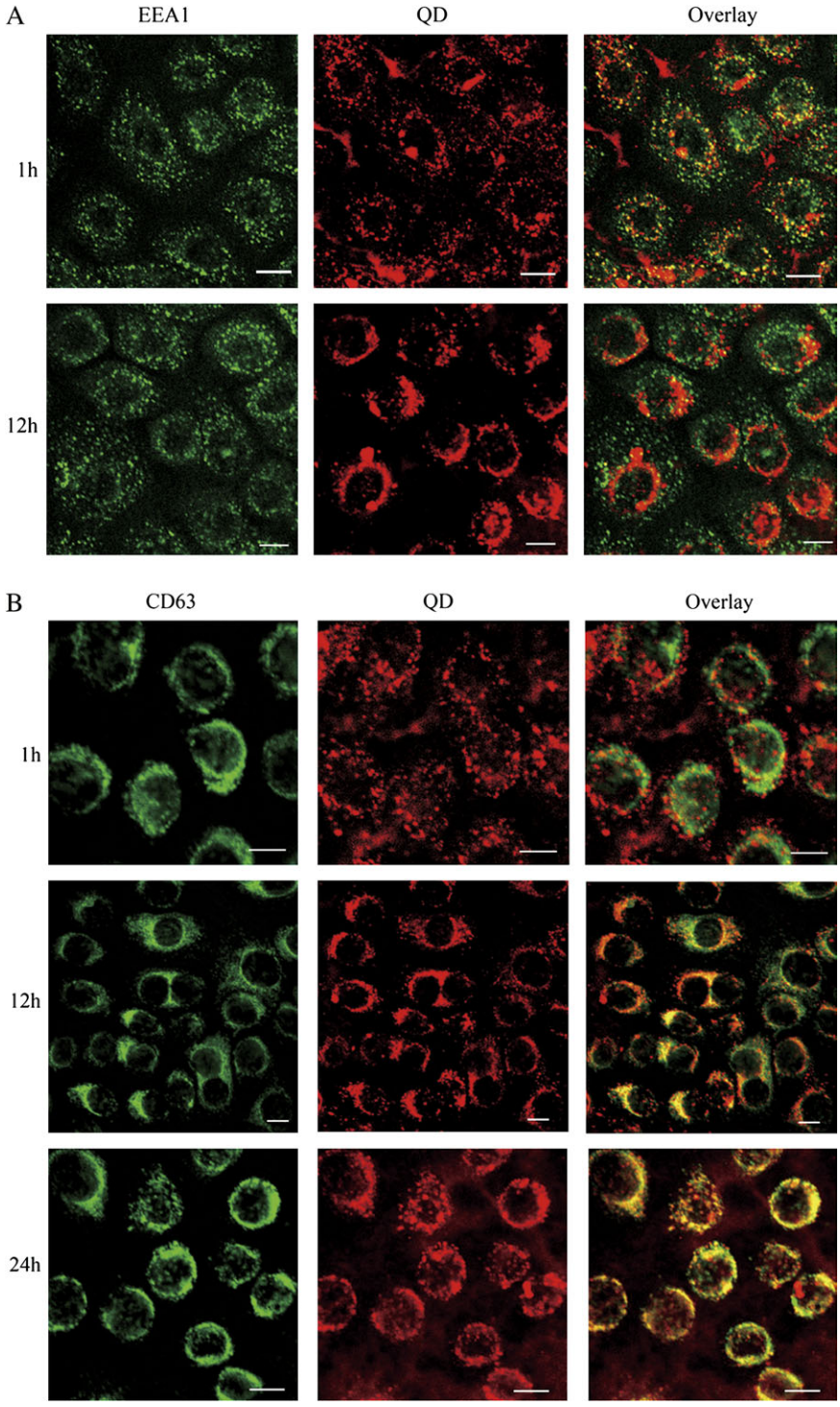

FIG. 4. QD colocalization with EEA1 or CD63. (A) EEA1 staining (green) of HEK with QD at 1 and 12 h. Note the QD distribution in HEK show a punctate pattern at 1 h and a perinuclear pattern at 12 h. Scale bar = 10 μm. (B) CD63 staining of HEK with QD at 1, 12, and 24 h. Scale bar = 10 μm.

which is typically a non-stable surface charge. Our colocalization and QD stability studies at different pHs suggest that QD could be stable and dispersed in early endosomes (near neutral pH), but more aggregated and fused in late endosomes/lysosomes due to the acidic pH.

Endosome and lysosome formation require microtubules to form a network in the cytoplasm, whereas actin generates forces to induce membrane invaginations (Cole and Lippincott-Schwartz, 1995; Schafer, 2002). To evaluate the cytoskeletal effects associated with QD endocytosis, we used four different

filament interfering agents. CytD disrupted F-actin filaments via actin depolymerization. However, the uptake of QD was not inhibited but slightly induced, and QD localization in early endosome was not affected (Fig. 6A). Y-27632, a specific inhibitor of Rho-associated kinase (ROCK) that can inhibit actin stress fiber formation (Katoh *et al*., 2001), did not inhibit QD uptake and influence its initial localization in early endosome (Fig. 6A). Genistein, a tyrosine kinase inhibitor that inhibits actin recruitment in caveolae (Rejman *et al*., 2005) did not inhibit QD uptake (Supplementary Table 2). Only nocodazole, a microtubule inhibitor, was found to decrease QD uptake and QD colocalization with EEA1 by CLSM (Fig. 6B). With FCM, nocodazole showed a significant reduction in QD uptake with a dose-dependent inhibitory effect (Fig. 6C). These results suggest that QD endocytosis is independent of F-actin and caveolae, but requires microtubules.

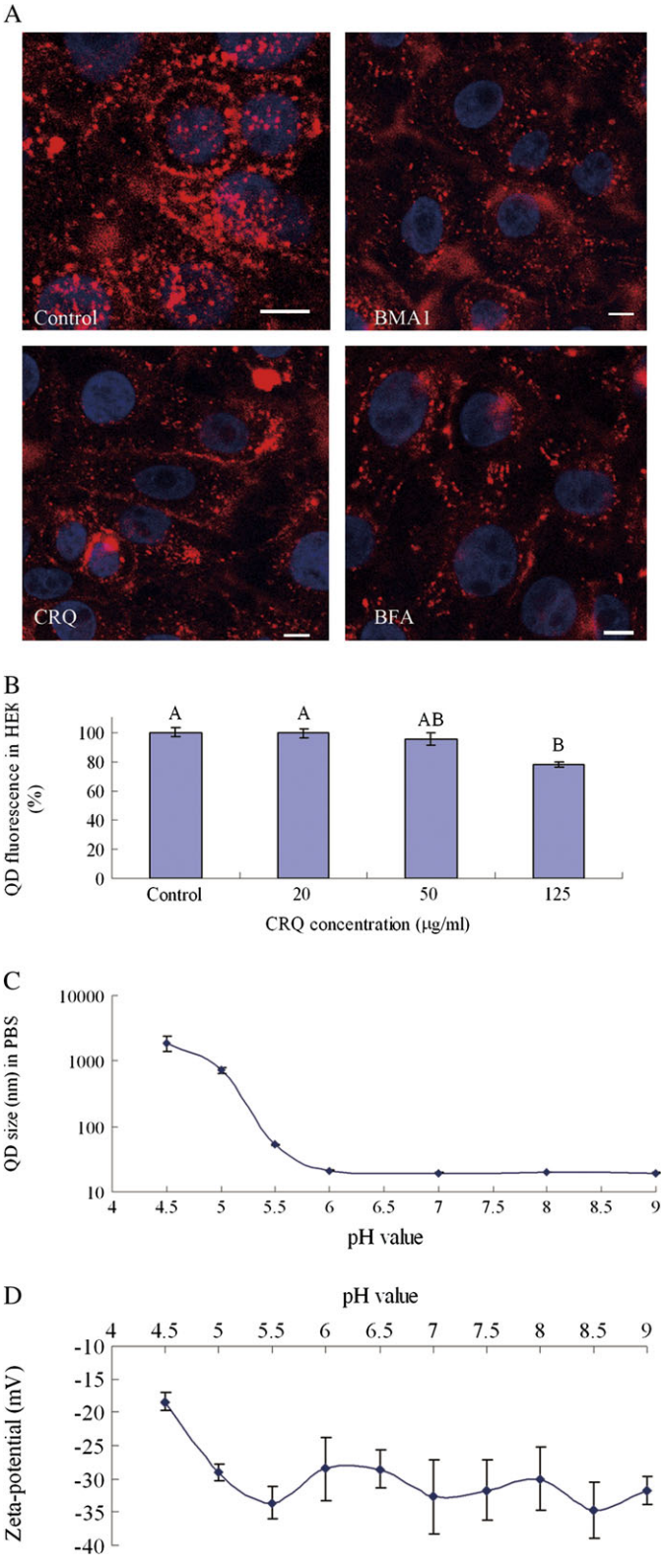

FIG. 5. QD uptake inhibition by endosome interfering reagents. (A) QD uptake inhibition by endosome interfering reagents of BMA1, CRQ or BFA at 30 min and visualized by CLSM. Scale bar = 10 μm. (B) Dose-dependent QD uptake inhibitory effects with CRQ. The QD fluorescence associated with cells was quantified by FCM compared with controls and the Mean ± SE are the average of duplicates ($p < 0.05$, Tukey HSD test). Histogram with different letters (A and B) denote mean values that are statistically different at $p < 0.05$. (C) QD size in PBS at different pHs. Error bars ± SE, $n = 7$. (D) QD zeta-potential in PBS at different pHs. Error bars ± SE, $n = 7$.

Regulation of QD Endocytosis by GPCR

To determine if a more specific endocytic pathway was involved, another QD with three different surface coatings with an emission of 565 nm was used as an inhibitor to investigate whether QD uptake was receptor mediated. QD565 coated with PEG, PEG-NH_2, or COOH was preincubated with HEK at 4nM. One hour later, QD (QD655-COOH, same as previous QD) was added to each of the three QD565 surface coatings for 30 min. As shown in Figure 7A, neither QD565-PEG nor QD565-NH_2 at 4nM inhibited QD uptake, whereas QD565-COOH at 4, 10, and 25nM were capable of reducing the QD uptake in a concentration-dependent manner. At the highest concentration of 25nM of QD565-COOH, QD were internalized slightly by HEK (7.88%), demonstrating that the surface coating of the QD rather than the core/shell complex determines QD uptake. These results suggest that a more specific pathway may be involved in QD recognition and internalization. Therefore, we investigated GPCR, a more specific receptor-mediated endocytic pathway. GPCR belongs to the largest family of membrane bound receptors and are targets of many drugs, and could play a role in QD endocytosis. We studied the effects of GPCR-related pathway using PTX, CTX, U-73122, and SRP because they are inhibitor of $G\alpha_i$-protein (G protein α subunit i family), $G\alpha_{t/s}$-protein activator, inhibitor of phospholipase C (PLC), and the inhibitor of protein kinase C (PKC) respectively. PTX but not CTX, reduced QD uptake, whereas U-73122 strongly blocked QD uptake as visualized by CLSM (Fig. 7B). QD inhibition by U-73122 was dose dependent and showed a significant decrease to 42.3% at 10 μg/ml compared with controls (Fig. 7C). In comparison,

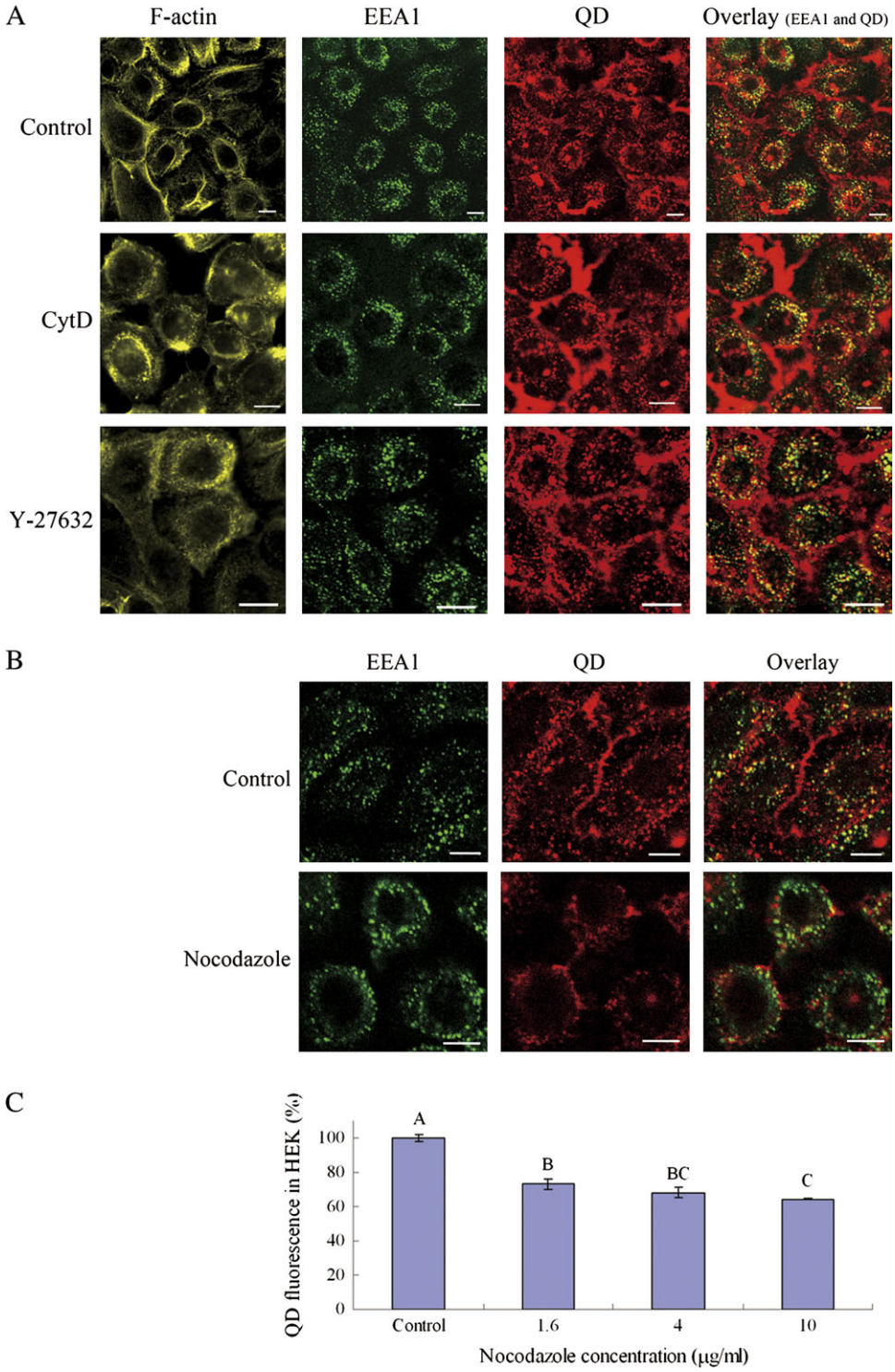

FIG. 6. QD uptake inhibition by cytoflilament disruptions. (A) QD uptake inhibition by CytD and Y-27632. F-actin was stained by Bodipy FL phallacidin (yellow, left column). Note that CytD and Y-27632 depolymerized F-actin. EEA1 as an early endosome marker is labeled (green). Scale bar = 10 μm. (B) QD uptake inhibition by nocodazole at 30 min. EEA1 staining (green) of HEK is shown. Scale bar = 10 μm. (C) QD uptake inhibitory effects by nocodazole at different concentrations. HEK were preincubated with nocodazole with indicated concentrations, and then QD applied to HEK for 30 min. QD fluorescence associated with cells was quantified by FCM. Mean ± SE are the average of duplicates ($p < 0.05$, Tukey HSD Test). Histogram with different letters (A, B, and C) denote mean values that are statistically different at $p < 0.05$.

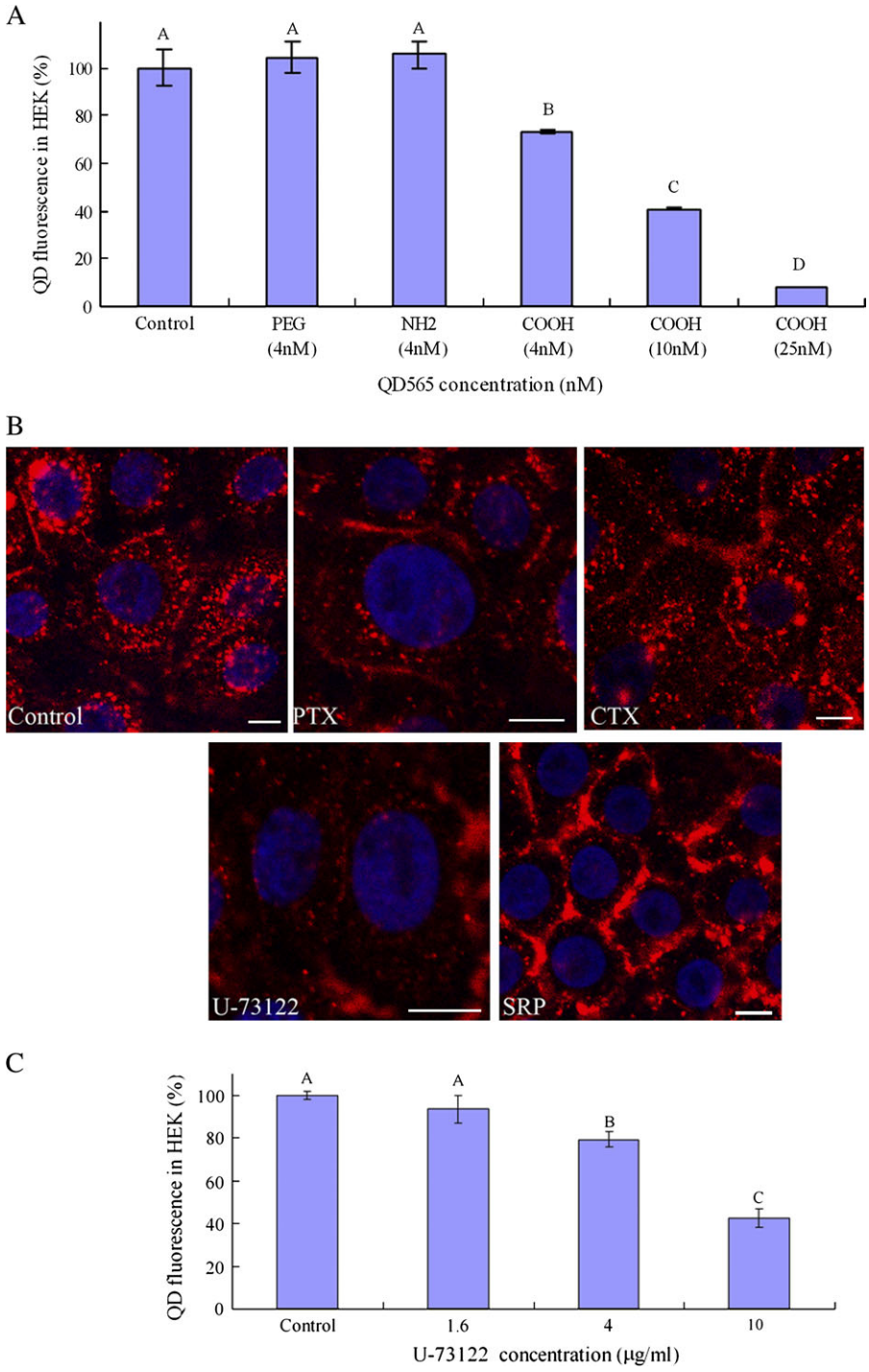

FIG. 7. QD uptake is receptor recognized and involved in GPCR-associated pathway. (A) QD655-COOH uptake inhibition with QD565 with different coatings at 30 min. Mean ± SE are the average of duplicates ($p < 0.05$, Tukey HSD Test). Histogram with different letters (A, B, C, and D) denote mean values that are statistically different at $p < 0.05$. (B) QD uptake inhibition by GPCR associated pathway inhibitors at 30 min. PTX, CTX, U-73122, and SRP are the inhibitor of Gαi-protein (G-protein α subunit i family), Gαt/s-protein activator, inhibitor of phospholipase C (PLC), and the inhibitor of PKC, respectively. Scale bar = 10 μm. (C) Dose-dependent QD uptake inhibitory effects with U-73122. HEK were preincubated with indicated concentrations of U-73122 for 1 h, and then incubated by 4nM of QD plus the inhibitor for 30 min. The QD fluorescence associated with cells was quantified by FCM compared with controls. Histogram with different letters (A, B, and C) denote mean values that are statistically different at $p < 0.05$.

SRP induced the QD uptake detected by FCM (125.9%, Supplementary Table 2). However, the small increase in uptake of the QD by SRP was probably due to an increase in large amounts of QD agglomerates at the periphery of the cells when visualized by CLSM but showing less fluorescence in the cell cytoplasm compared with controls (Fig. 7B).

LDL/Scavenger Receptors in QD Uptake

These above results suggest QD endocytosis is regulated by the GPCR-associated pathway and may be receptor-specific. Recently, low-density lipoprotein receptors (LDLRs) were found to induce PKC translocation to plasma membrane via $G\alpha_i$ protein (Heo *et al*., 2008). LDLR or scavenger receptors (SRs) recognize and regulate LDL or acetylated low-density lipoprotein (AcLDL) uptake. It has been determined that the size of human LDL is 24–26 nm (Yamane *et al*., 1996). Our study also showed that the hydrodynamic size of QD in KGM-2 measured by DLS was 27.5 nm (Table 2), similar to the size of LDL (28.2 nm) or AcLDL (28.1 nm), suggesting the potential for SR/LDLR recognition for QD uptake. Scavenger receptor class B type I (SR-BI) recognized the AcLDL, which is negatively charged (Fukasawa *et al*., 1995) and is similar to the QD used in this study (Fig. 5D). In addition, LDLR and SC-BI are present in HEK (te Pas *et al*., 1991; Tsuruoka *et al*., 2002). We hypothesized that LDLR and SR-BI may play a role in QD endocytosis due to the similar size/charge of LDL/AcLDL with QD, and the link with GPCR-associated proteins. Therefore, the inhibitors of the SR such as polyI or FCD were studied. Scavenger receptor inhibitors strongly reduced the uptake of QD in CLSM (Fig. 8A). Inhibition by polyI and FCD showed a strong inhibitory effect when evaluated by FCM (Supplementary Table 2). We also used the LDL and AcLDL which served as ligands for LDLR/SR to observe if they could compete with QD and block QD uptake. LDL strongly reduced the QD fluorescence in HEK, and AcLDL showed less competition with QD in CLSM (Fig. 8A). The inhibitory effects by both proteins were dose dependent, whereas BSA at 25 μg/ml served as the protein control and did not show any inhibitory effect (Fig. 8B).

QD Uptake by Macropinocytosis and HEK Pathways

The macropinocytosis pathway was investigated by using four inhibitors. The inhibitor 5-(N,N-dimethyl)-amiloride (DMA) is a Na^+/H^+ exchanger that slightly reduced QD uptake to 87.58% compared with controls, whereas QD distribution by CLSM were similar to the controls. Phosphoinositide 3-kinase (PI3K) is a key kinase for regulating macropinocytosis and can be inhibited by Ly294002 (LY) and wortmannin (WMN) (Araki *et al*., 1996). No inhibitory effects were noted with either of these inhibitors. NaN_3, which was thought to play a preferable role in macropinocytosis (Chen *et al*., 2006), inhibited the QD uptake by coincubation (77.88%) but not by the preincubation method (Supplementary Table 2). QD uptake reduction by NaN_3 coincubation with QD was probably due to QD degradation in the KGM-2 by NaN_3 (Supplementary Table 1). These results suggest that macropinocytosis is not involved in QD uptake pathways.

We also studied whether QD could be internalized into cells via the melanosome-transfer pathway, which is specific for HEK (Sharlow *et al*., 2000). Y-27632, TrpI, and NCM can inhibit melanosome transfer into keratinocytes (Hakozaki *et al*., 2002; Scott *et al*., 2003; Seiberg *et al*., 2000). However, Y-27632, TrpI, and NCM did not inhibit QD uptake visualized by CLSM and quantified by FCM (Supplementary Table 2).

QD Toxicity on HEK and the Cytoskeleton

The toxicity of QD should be considered as protein markers in biomedical applications. Monteiro-Riviere *et al*. (2009) showed that neither low (2nM) nor high (20nM) concentrations of QD decrease HEK viability when evaluated by the cell titer blue assay and cell titer 96 AQ assay (Promega Corp., Madison, WI) at 24 h. However, when using the 3-(4,5-dimethylthiazol-2-yl)-2,5-diphenyltetrazolium bromide assay, QD toxicity showed a statistically significant decrease at high concentrations. In our study, the live/dead cell assay was used to assess QD toxicity. After 24 h of QD (20nM) incubation, no dead cells were noted but the morphology of HEK appeared more spherical compared with controls, whereas at 48 h of incubation slight cell death with EthD-1 staining (red) was noted and calcein AM green staining was less compared with controls (Fig. 9A). In addition, there was an increase in F-actin stress fibers at 20nM of QD at 24 h (Fig. 9B), suggesting long term incubation of QD can alter the cytoskeleton staining pattern, which is different from cadmium toxicity that induces F-actin depolymerization (Mills and Ferm, 1989). Although the QD toxicity in HEK was low and dependent on the assay used, the detectable F-actin change in morphology may alter the structure of cells thereby compromising experimental results.

TABLE 2
The Size (nm) of QD, LDL, AcLDL in water or KGM-2

	QD655-COOH	LDL	AcLDL
Water	21.94 ± 0.97	25.72 ± 0.6	27.56 ± 0.88
KGM-2	27.54 ± 0.13	28.24 ± 0.24	28.11 ± 0.26

DISCUSSION

In summary, a figure of a cell is provided to illustrate the potential pathways for the QD uptake mechanism (Fig. 10). This indicates the inhibitors used and their effectors, and QD intracellular localization and translocation within the cytoplasm. The carboxylic QD are capable of internalizing into the cells rather quickly and this endocytosis process could be dependent on lipid rafts and the GPCR pathway (labeled in green). The

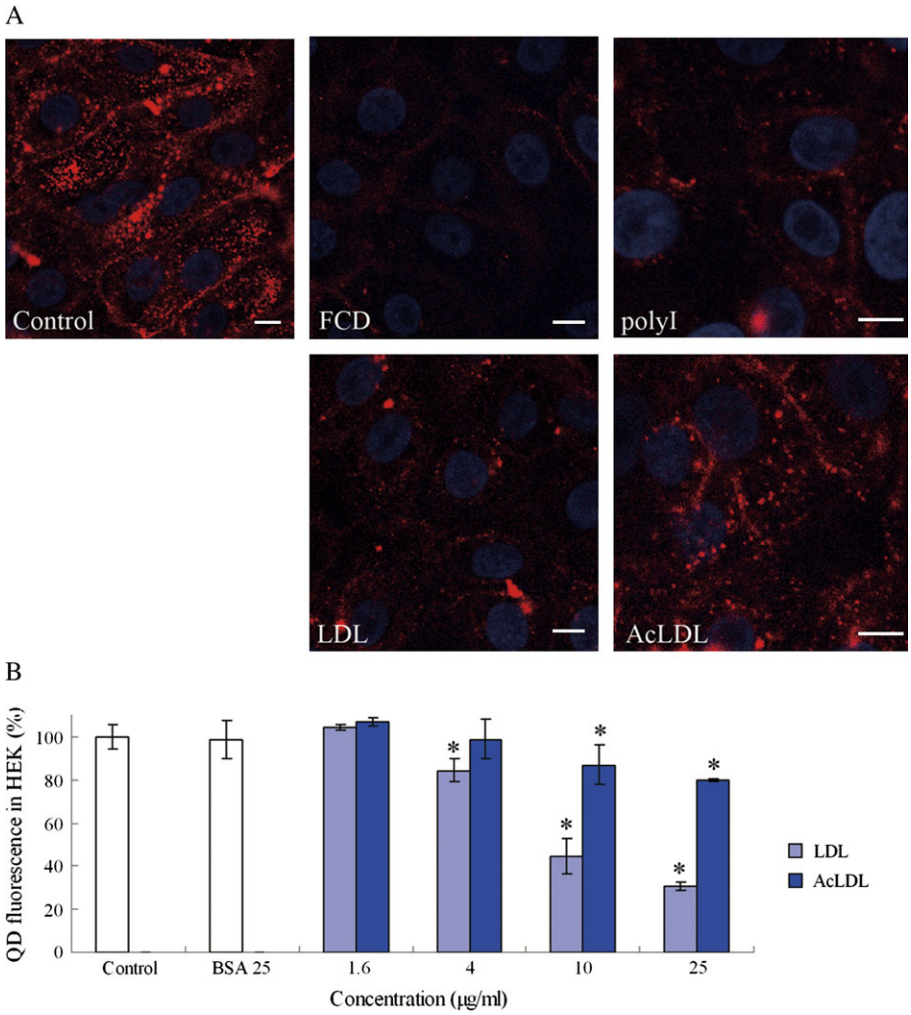

FIG. 8. Scavenger receptor are involved in QD uptake. (A) QD uptake inhibition by scavenger receptor inhibitors of polyI and FCD, or receptor ligands of LDL and AcLDL, and were present by CLSM. (B) QD uptake inhibitory effects by receptor ligands (LDL or AcLDL) and bovine serum albumin (BSA) control. Mean ± SE are the average of duplicates ($p < 0.05$, Tukey HSD Test). *Indicates statistically significant difference from control.

precise uptake mechanism for other nanomaterials or NP may still be unknown but for QD655-COOH is primarily recognized by the LDLR/SR-BI. Also, it is believed that the surface coatings and charge could be the key determinant for NP to be recognized by certain receptor(s). Carboxylic acid–coated QD with different emission wavelengths can be conjugated with active molecules to target specific proteins in cells. It has been thought that only the surface conjugations of peptide/antibody/RNA determined the endocytic pathways. However, there is concern that if this conjugation is not efficient, the ability of QD to penetrate cells and nanoparticle targeting may be influenced by the unconjugated areas or the surface coating itself. In addition, due to the cytotoxicity seen and the increase in F-actin stress fibers by QD, suggest that QD may not be ideal to target proteins in live cells for long-term use.

Most of the protein/macromolecule endocytosis depends on clathrin-mediated endocytosis, in which the adaptor proteins (AP-2 and eps15) are required for clathrin pit formation (Benmerah *et al.*, 1998; Tebar *et al.*, 1996). Several types of NP such as SPION (FITC labeled, 50 nm) and PEG-PLA of ~90 nm have been shown to enter cells via this pathway (Harush-Frenkel *et al.*, 2008; Lu *et al.*, 2007). Our results clearly show that QD uptake was clathrin independent based on the following reasons: (1) no colocalization was found between QD and clathrin at 1 h; (2) staining of eps15, a clathrin adaptor protein (Sieczkarski and Whittaker, 2002), did not colocalize with QD; (3) CPM, a cationic amphiphilic drug used to prevent clathrin-mediated virus endocytosis by disrupting the assembly of the clathrin pits on the cell surface (Stuart and Brown, 2006; Wang *et al.*, 1993), did not inhibit QD endocytosis. Instead, QD colocalized partially with caveolin 1 and the uptake was sensitive to cholesterol removal reagents such as MβCD and lovastatin (Fig. 3C). Clathrin pits are 120 nm in size, whereas caveolae are smaller ~60 nm in size (Conner and Schmid, 2003). The well-dispersed QD in KGM-2 cell medium may be recognized partially by caveolae due to its smaller size that

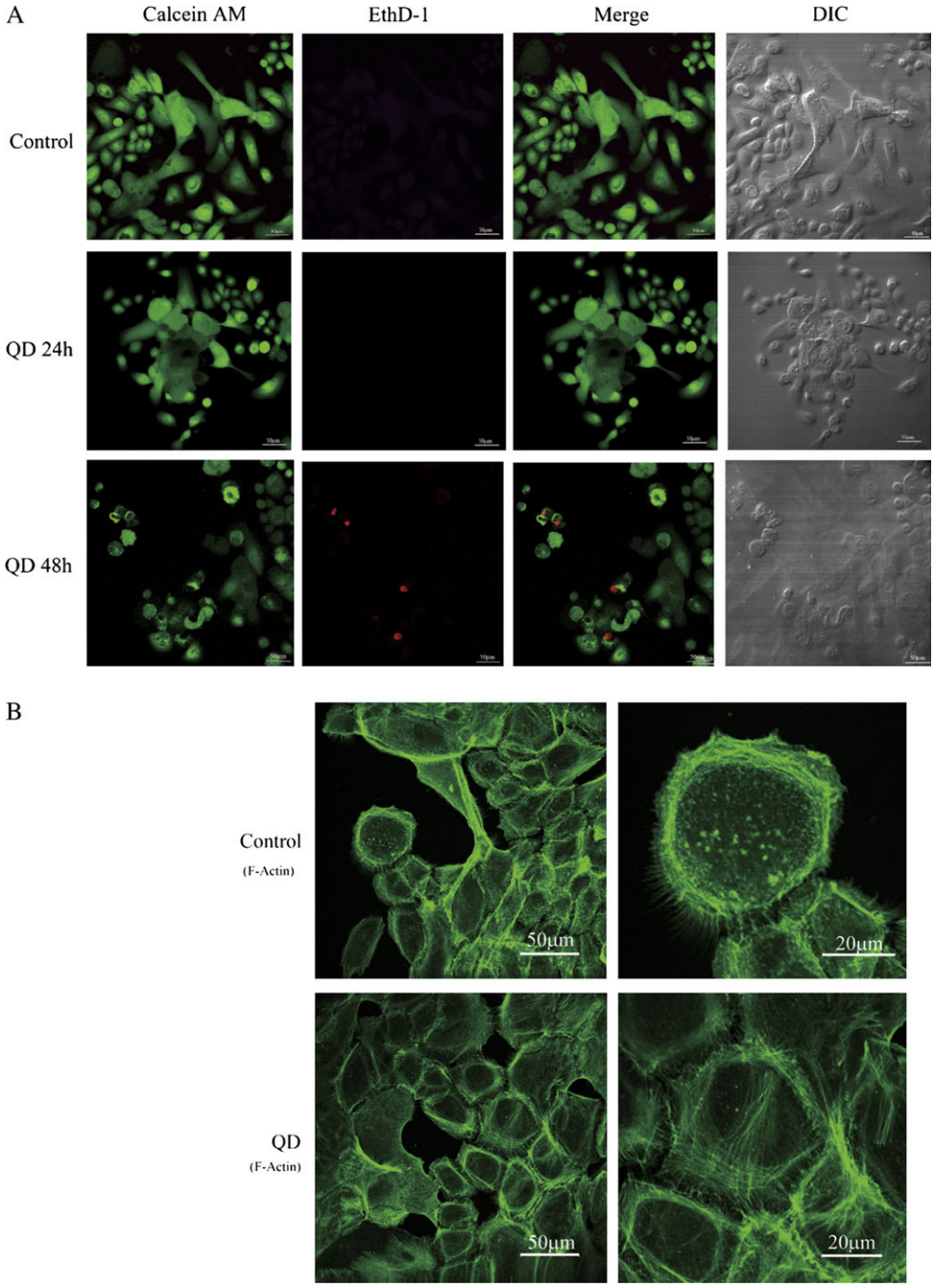

FIG. 9. QD present minor but long-term cytotoxicity. (A) QD cytotoxicity evaluated by Live/Dead assay. HEK were incubated with 20nM of QD for 24 and 48 h. The cells were incubated with 1μM calcein AM/2μM EthD-1 for 30 min. The fluorescence of calcein AM (green, left column), EthD-1 (red, second column), overlay (third column), and DIC mode (fourth column) are shown. Scale bar = 50 μm.

may wrap the individual QD tightly. The minor colocalization of QD with caveolin 1, and the slow internalization of caveolae (Conner and Schmid, 2003), indicate the QD uptake may be regulated via caveolae partially participated through cholesterol dependent routes. Therefore, lipid rafts mediated endocytosis was taken into account. Raft mediated endocytosis can lead to rapid ligand uptake that can be restored within 30 min after a change of environment (Damke *et al*., 1995). Our negatively charged QD rapidly became internalized into HEK at 5 min, suggesting a raft mediated pathway involvement. CTB is a nontoxic cell-binding moiety that interacts with gangliosides GM1 on the surfaces of mammalian cells, and its conjugation with different types of fluorochromes was used as a marker for lipid rafts (Harder *et al*., 1998; Janes *et al*., 1999; Wang *et al*.,

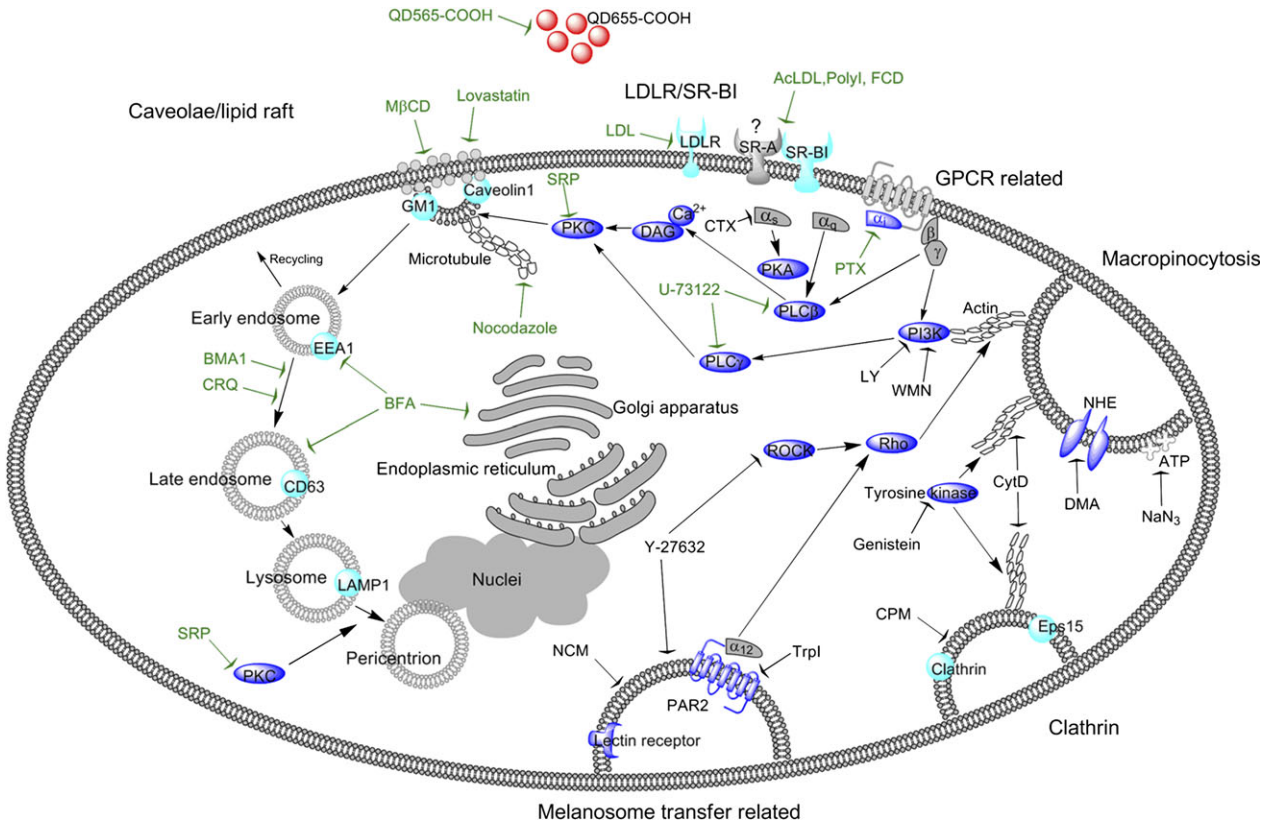

FIG. 10. QD nanoparticle endocytic pathway. QD uptake mechanism and subcellular localization with 24 inhibitors with different inhibitory functions and protein markers for organelles. Lipid rafts, caveolin 1, clathrin, early endosome, late lysosomes are stained (teal). Inhibitors are located near the targets where they exert their functions. Inhibitory effects are labeled in green, whereas no inhibitory effects are labeled in black. Briefly, QD were first recognized by lipid rafts (CTX as marker, which binds to ganglioside GM1) and get internalized into early endosome (EEA1 as the marker), then localized in late endosome (CD63) and remained in the lysosome (LAMP1). QD uptake was through the GPCR and the downstream proteins regulated by G_i protein, PLC, and PKC. These inhibitors blocked QD uptake, indicating QD endocytosis may be recognized by specific receptors. The inhibitors for scavenger receptors (polyI and FCD) greatly blocked QD. LDL/AcLDL competed with QD and reduced QD internalization suggesting that LDLR/SR-BI may be the most appropriate receptors of QD uptake.

2006). QD were found to colocalize with CTB at the cell periphery by 15 min and in the cytoplasm by 30 min, suggesting the QD uptake pathway is mediated by lipid rafts (Fig. 3B). It has been reported that positively charged particles can internalize into cells via the clathrin-mediated pathway. Positive charged mesoporous silica NP of 110 nm were taken up by 3T3-L1 mouse embryonic cells and hMSC via clathrin and actin dependent endocytosis (Chung *et al.*, 2007). Also, positively charged D,L-PLA-NP was found to enter Hela cells via clathrin-mediated endocytosis (Harush-Frenkel *et al.*, 2007). Our laboratory has shown that the carboxylic acid–coated QD565 were present in greater number than QD655 in HEK. However, our results depicted that the negatively charged QD uptake was lipid raft mediated, which is different from the uptake of positively charged NP that are clathrin dependent.. However, the exact relationship between NP surface charges and pathways (clathrin or caveolae) is unknown and needs further clarification.

Little is known whether NP can be recognized and internalized by specific cell membrane receptors that behave similar to receptor bound ligands and some viruses. GPCR are the largest family of membrane bound receptors and can be coupled to the activation of phospholipase Cβ (PLC-β), which can increase calcium concentration and PKC activation, through G proteins of the α_q family (G-α_q) (Dorsam and Gutkind, 2007), whereas $G_{\beta\gamma}$ subunit released from G$\alpha_{i/o}$ can also activate PLCβ (Rebecchi and Pentyala, 2000). QD uptake was attenuated by PTX, $G_{\alpha i}$ inhibitor, and by U-73122, a PLC inhibitor, suggesting the role of G_i protein and its downstream effector phospholipase in regulating QD uptake. SRP is a microbial alkaloid with activity against a variety of protein kinases, including PKC and PKA (Swannie and Kaye, 2002). SRP did not show the inhibition of cell-associated QD uptake evaluated by FCM, but QD accumulation with a large amount was seen along the periphery of the cell membrane but not in the cytoplasm (Fig. 7B). PKC regulates the internalization and trafficking of numerous plasma membrane proteins, and sequesters caveolin to the pericentrion, the juxtanuclear compartments (Idkowiak-Baldys *et al.*, 2006). Thus, PKC activity disruption may block QD movement to perinuclear

compartments, thereby leads to QD accumulation near the periphery of the cells that could be similar to the adenovirus after PKC inhibition (Nakano *et al*., 2000).

Based on the finding that QD uptake was regulated by several key proteins in GPCR-associated pathways, we hypothesized that QD internalization may require a specific pathway. Studies have reported that acetylated and oxidized LDL NP uptake by macrophages was class A scavenger receptor mediated and PTX-sensitive (Chang *et al*., 2008; Whitman *et al*., 2000). Oxidized LDL was capable of inhibiting hepatitis C virus entry in human hepatoma cells and SR-BI is an essential component of the receptor complex for the virus (von Hahn *et al*., 2006). SR-BI recognized the acetylated low-density lipoproteins (AcLDL) and phosphatidylserine-containing liposomes (PS-liposomes), which are both negatively charged (Fukasawa *et al*., 1995, 1996). In addition, LDL was later localizing in endosome-lysosomal compartments (Maxfied and Wüstner, 2002). LDLR and SC-BI are present in HEK (Ponec *et al*., 1992; Tsuruoka *et al*., 2002), whereas CD36, another type of SC-B, was not expressed in normal HEK (Alessio *et al*., 1998) and SC-A expression was not reported. Inhibitors of SR (polyI and FCD) and receptor ligands (LDL or AcLDL) significantly blocked QD uptake (Fig. 8A), suggesting the LDL/SR pathway was strongly involved in QD uptake. The fact that QD could be recognized by LDLR/SR, lipid raft dependent and GPCR pathway regulated, indicated that QD uptake may differ from the uptake mechanism of other larger NP, that normally occurs through the clathrin mediated pathway, or macropinocytosis primarily if the NP is greater than 200 nm (Harush-Frenkel *et al*., 2007; Khalil *et al*., 2007).

HEK are skin cells which are involved in melanosome uptake pathway via the phagocytosis pathway, which is mainly regulated by PAR-2, a member of GPCR (Sharlow *et al*., 2000). Receptors that transmit signals through heterotrimeric G proteins activate Rho-dependent pathways through a variety of signaling intermediates (Fukuhara *et al*., 1999). Further, PAR-1 receptor signaling has been linked to Rho through the pertussis-toxin insensitive $G_{12}\alpha$ family of proteins (Majumdar *et al*., 1998; Martin *et al*., 2001). Phagocytosis is Rho protein dependent and can be blocked by *difficile* toxin B or Y-27632, inhibitors of Rho or its kinase (Scott *et al*., 2003). Serine protease inhibitors that interfere with PAR-2 activation, such as the soybean TrpI, induced depigmentation of the skin (Seiberg *et al*., 2000). In addition, NCM is a biologically active form of niacin (vitamin B3) that effectively inhibits melanosome transfer in melanocyte-keratinocyte co-culture model system (Hakozaki *et al*., 2002). However, Y-27632, TrpI, and NCM did not block the QD uptake, indicating that the melanosome-transfer like independent pathways were not involved in NP endocytosis.

QD could internalize in cells like some virus particles because they are similar in size. Beer and Pedersen (2006) found that NIH3T3 cells took up amphotropic murine leukemia virus by attaching to large rafts where the caveolin 1 was not enriched, which is similar to the QD endocytic pathway. Therefore, it would be of interest to compare the endocytic pathways of this virus to that of the QD pathways presented in this paper to determine a possible linkage between the "lifeless" and living matters. However, the leukemia virus is 110 nm, which is different from our QD, which was 27 nm in the culture medium. Small round viruses of 18–24 nm (Saif *et al*., 1990), picorna-like virus of 30 nm (Wang *et al*., 1999), and *M. rosenbergii* nodavirus of 30 nm (Arcier *et al*., 1999), could follow the same mechanistic pathways as our QD due to size.

Finally, we cannot generalize that all NP will follow these pathways or even state that all negatively charge NP will be involved in these specific pathways. The data reported here does indicate that cellular internalization can be prevented using different endocytic inhibitory agents. Also, we have shown that QD655 with a carboxylic acid coating is regulated primarily by the LDLR/SR pathway and the G-protein–coupled receptor associated pathway is also involved. This study provides insight that the surface charge and size are determinant factors that may play a major role in understanding the cellular mechanism of QD NP uptake in cells.

SUPPLEMENTARY DATA

Supplementary data are available online at http://toxsci.oxfordjournals.org/.

FUNDING

United States Air Force Office of Scientific Research (AFOSR) Grant (FA9550-08-1-0182).

ACKNOWLEDGMENTS

This work was presented at the 48th Annual Meeting of the Society of Toxicology, Baltimore, Maryland in March 2009.

REFERENCES

Alessio, M., Gruarin, P., Castagnoli, C., Trombotto, C., and Stella, M. (1998). Primary ex vivo culture of keratinocytes isolated from hypertrophic scars as a means of biochemical characterization of CD36. *Int. J. Clin. Lab. Res.* **28,** 47–54.

Araki, N., Johnson, M. T., and Swanson, J. A. (1996). A role for phosphoinositide 3-kinase in the completion of macropinocytosis and phagocytosis by macrophages. *J. Cell Biol.* **135,** 1249–1260.

Arcier, J. M., Herman, F., Lightner, D. V., Redman, R. M., Mari, J., and Bonami, J. R. (1999). A viral disease associated with mortalities in hatchery-reared postlarvae of the giant freshwater prawn Macrobrachium rosenbergii. *Dis. Aquat. Org.* **38,** 177–181.

Asokan, A., and Cho, M. J. (2002). Exploitation of intracellular pH gradients in the cellular delivery of macromolecules. *J. Pharm. Sci.* **91,** 903–913.

Beer, C., and Pedersen, L. (2006). Amphotropic murine leukemia virus is preferentially attached to cholesterol-rich microdomains after binding to mouse fibroblasts. *Virol. J.* **3,** 21.

Benmerah, A., Lamaze, C., Bègue, B., Schmid, S. L., Dautry-Varsat, A., and Cerf-Bensussan, N. (1998). AP-2/Eps15 interaction is required for receptor-mediated endocytosis. *J. Cell. Biol.* **140,** 1055–1062.

Chang, C. L., Hsu, H. Y., Lin, H. Y., Chiang, W., and Lee, H. (2008). Lysophosphatidic acid-induced oxidized low-density lipoprotein uptake is class A scavenger receptor-dependent in macrophages. *Prostaglandins Other Lipid Mediat.* **87,** 20–25.

Chang, E., Thekkek, N., Yu, W. W., Colvin, V. L., and Drezek, R. (2006). Evaluation of quantum dot cytotoxicity based on intracellular uptake. *Small* **12,** 1412–1417.

Chen, J., Li, G., Lu, J., Chen, L., Huang, Y., Wu, H., Zhang, J., and Lu, D. (2006). A novel type of PTD, common helix-loop-helix motif, could efficiently mediate protein transduction into mammalian cells. *Biochem. Biophys. Res. Commun.* **347,** 931–940.

Cole, N. B., and Lippincott-Schwartz, J. (1995). Organization of organelles and membrane traffic by microtubules. *Curr. Opin. Cell Biol.* **7,** 55–64.

Conner, S. D., and Schmid, S. L. (2003). Regulated portals of entry into the cell. *Nature* **422,** 37–44.

Chung, T. H., Wu, S. H., Yao, M., Lu, C. W., Lin, Y. S., Hung, Y., Mou, C. Y., Chen, Y. C., and Huang, D. M. (2007). The effect of surface charge on the uptake and biological function of mesoporous silica NPs in 3T3-L1 cells and human mesenchymal stem cells. *Biomaterials* **28,** 2959–2966.

Damke, H., Baba, T., van der Bliek, A. M., and Schmid, S. L. (1995). Clathrin-independent pinocytosis is induced in cells overexpressing a temperature-sensitive mutant of dynamin. *J. Cell. Biol.* **131,** 69–80.

Dausend, J., Musyanovych, A., Dass, M., Walther, P., Schrezenmeier, H., Landfester, K., and Mailander, V. (2008). Uptake mechanism of oppositely charged fluorescent nanoparticles in HeLa cells. *Macromol. Biosci.* **8,** 1135–1143.

Derfus, A. M., Chan, W. C. W., and Bhatia, S. (2004). Probing the cytotoxicity of semiconductor nanocrystals. *Nano Lett.* **4,** 11–18.

Dorsam, R. T., and Gutkind, J. S. (2007). G-protein-coupled receptors and cancer. *Nat. Rev. Cancer* **7,** 79–94.

Duan, H., and Nie, S. (2007). Cell-penetrating quantum dots based on multivalent and endosome-disrupting surface coatings. *J. Am. Chem. Soc.* **129,** 3333–3338.

Ehrlich, M., Boll, W., Van Oijen, A., Hariharan, R., Chandran, K., Nibert, M. L., and Kirchhausen, T. (2004). Endocytosis by random initiation and stabilization of clathrin-coated pits. *Cell* **118,** 591–605.

Fukasawa, M., Hirota, K., Adachi, H., Mimura, K., Murakami-Murofushi, K., Tsujimoto, M., Arai, H., and Inoue, K. (1995). Chinese hamster ovary cells expressing a novel type of acetylated low density lipoprotein receptor. Isolation and characterization. *J. Biol. Chem.* **270,** 1921–1927.

Fukasawa, M., Adachi, H., Hirota, K., Tsujimoto, M., Arai, H., and Inoue, K. (1996). SRB1, a class B scavenger receptor, recognizes both negatively charged liposomes and apoptotic cells. *Exp. Cell. Res.* **222,** 246–250.

Fukuhara, S., Murga, C., Zohar, M., Igishi, T., and Gutkind, J. S. (1999). A novel PDZ domain containing guanine nucleotide exchange factor links heterotrimeric G proteins to Rho. *J. Biol. Chem.* **274,** 5868–5879.

Gao, X., Cui, Y., Levenson, R. M., Chung, L. W., and Nie, S. (2004). In vivo cancer targeting and imaging with semiconductor quantum dots. *Nat. Biotechnol.* **22,** 969–976.

Hakozaki, T., Minwalla, L., Zhuang, J., Chhoa, M., Matsubara, A., Miyamoto, K., Greatens, A., Hillebrand, G. G., Bissett, D. L., and Boissy, R. E. (2002). The effect of niacinamide on reducing cutaneous pigmentation and suppression of melanosome transfer. *Br. J. Dermatol.* **147,** 20–31.

Harder, T., Scheiffele, P., Verkade, P., and Simons, K. (1998). Lipid domain structure of the plasma membrane revealed by patching of membrane components. *J. Cell. Biol.* **141,** 929–942.

Harush-Frenkel, O., Debotton, N., Benita, S., and Altschuler, Y. (2007). Targeting of NPs to the clathrin-mediated endocytic pathway. *Biochem. Biophys. Res. Commun.* **353,** 26–32.

Harush-Frenkel, O., Rozentur, E., Benita, S., and Altschuler, Y. (2008). Surface charge of NPs determines their endocytic and transcytotic pathway in polarized MDCK cells. *Biomacromolecules* **9,** 435–443.

Heo, K. S., Kim, D. U., Kim, L., Nam, M., Baek, S. T., Park, S. K., Park, Y., Myung, C. S., Hwang, S. O., and Hoe, K. L. (2008). Activation of PKCbeta(II) and PKCtheta is essential for LDL-induced cell proliferation of human aortic smooth muscle cells via Gi-mediated Erk1/2 activation and Egr-1 upregulation. *Biochem. Biophys. Res. Commun.* **368,** 126–131.

Idkowiak-Baldys, J., Becker, K. P., Kitatani, K., and Hannun, Y. A. (2006). Dynamic sequestration of the recycling compartment by classical protein kinase C. *J. Biol. Chem.* **281,** 22321–22331.

Invitrogen website Quantum dots & microspheres. (2009). http://www.invitrogen.com/site/us/en/home/Products-and-Services/Applications/Cell-and-Tissue-Analysis/qdots-microspheres-nanospheres.html.

Jaiswal, J. K., Mattoussi, H., Mauro, J. M., and Simon, S. M. (2003). Long-term multiple color imaging of live cells using quantum dot bioconjugates. *Nat. Biotechnol.* **21,** 47–51.

Janes, P. W., Ley, S. C., and Magee, A. I. (1999). Aggregation of lipid rafts accompanies signaling via the T cell antigen receptor. *J. Cell. Biol.* **147,** 447–461.

Jordan, A., Scholz, R., Wust, P., Schirra, H., Thomas, S., Schmidt, H., and Felix, R. (1999). Endocytosis of dextran and silan-coated magnetite NPs and the effect of intracellular hyperthermia on human mammary carcinoma cells in vitro. *J. Magn. Magn. Mater.* **194,** 185–196.

Katoh, K., Kano, Y., Amano, M., Onishi, H., Kaibuchi, K., and Fujiwara, K. (2001). Rho-kinase–mediated contraction of isolated stress fibers. *J. Cell. Biol.* **153,** 569–584.

Khalil, I. A., Kogure, K., Futaki, S., Hama, S., Akita, H., Ueno, M., Kishida, H., Kudoh, M., Mishina, Y., Kataoka, K., *et al.* (2007). Octaarginine-modified multifunctional envelope-type NPs for gene delivery. *Gene Ther.* **14,** 682–689.

Lajoie, P., and Nabi, I. R. (2007). Regulation of raft-dependent endocytosis. *J. Cell. Mol. Med.* **11,** 644–653.

Lu, C. W., Hung, Y., Hsiao, J. K., Yao, M., Chung, T. H., Lin, Y. S., Wu, S. H., Hsu, S. C., Liu, H. M., Mou, C. Y., *et al.* (2007). Bifunctional magnetic silica NPs for highly efficient human stem cell labeling. *Nano Lett.* **7,** 149–154.

Mailander, V., Lorenz, M. R., Holzapfel, V., Musyanovych, A., Fuchs, K., Wiesneth, M., Walther, P., Landfester, K., and Schrezenmeier, H. (2008). Carboxylated superparamagnetic iron oxide particles label cells intracellularly without transfection agents. *Mol. Imaging Biol.* **10,** 138–146.

Majumdar, M., Seasholtz, T. M., Goldstein, D., de Lanerolle, P., and Brown, J. H. (1998). Requirement for Rho-mediated myosin light chain phosphorylation in thrombin-stimulated cell rounding and its dissociation from mitogenesis. *J. Biol. Chem.* **273,** 10099–10106.

Martin, C. B., Mahon, G. M., Klinger, M. B., Kay, R. J., Symons, M., Der, C. J., and Whitehead, I. P. (2001). The thrombin receptor, PAR-1, causes transformation by activation of Rho-mediated signaling pathways. *Oncogene* **20,** 1953–1963.

Maxfield, F. R., and Wüstner, D. (2002). Intracellular cholesterol transport. *J. Clin. Invest.* **110,** 891–898.

Michalet, X., Pinaud, F. F., Bentolila, L. A., Tsay, J. M., Doose, S., Li, J. J., Sundaresan, G., Wu, A. M., Gambhir, S. S., and Weiss, S. (2005). Quantum dots for live cells, in vivo imaging, and diagnostics. *Science* **307,** 538–544.

Mills, J. W., and Ferm, V. H. (1989). Effect of cadmium on F-actin and microtubules of Madin-Darby canine kidney cells. *Toxicol. Appl. Pharmacol.* **101,** 245–254.

Monteiro-Riviere, N. A., Nemanich, R., Inman, A., Wang, Y., and Riviere, J. (2005). Multi-walled carbon nanotube interactions with human epidermal keratinocytes. *Toxicol. Lett.* **155,** 377–384.

Monteiro-Riviere, N. A., Inman, A., and Zhang, L. W. (2009). Limitations and relative utility of screening assays to assess engineered nanoparticle toxicity in a human cell line. *Toxicol. Appl. Pharmacol.* **234,** 222–235.

Mukherjee, S., Ghosh, R. N., and Maxfield, F. R. (1997). Endocytosis. *Physiol. Rev.* **77,** 759–803.

Nakano, M. Y., Boucke, K., Suomalainen, M., Stidwill, R. P., and Greber, U. F. (2000). The first step of adenovirus type 2 disassembly occurs at the cell surface, independently of endocytosis and escape to the cytosol. *J. Virol.* **74,** 7085–7095.

Nichols, B. (2003). Caveosomes and endocytosis of lipid rafts. *J. Cell. Sci.* **116,** 4707–4714.

Pelkmans, L., Püntener, D., and Helenius, A. (2002). Local actin polymerization and dynamin recruitment in SV40-induced internalization of caveolae. *Science* **296,** 535–539.

Ponec, M., te Pas, M. F., Havekes, L., Boonstra, J., Mommaas, A. M., and Vermeer, B. J. (1992). LDL receptors in keratinocytes. *J. Invest. Dermatol.* **98,** 50S–56S.

Qaddoumi, M. G., Ueda, H., Yang, J., Davda, J., Labhasetwar, V., and Lee, V. H. (2004). The characteristics and mechanisms of uptake of PLGA NPs in rabbit conjunctival epithelial cell layers. *Pharm. Res.* **4,** 641–648.

Rebecchi, M. J., and Pentyala, S. N. (2000). Structure, function, and control of phosphoinositide-specific phospholipase C. *Physiol. Rev.* **80,** 1291–1335.

Rejman, J., Bragonzi, A., and Conese, M. (2005). Role of clathrin- and caveolae-mediated endocytosis in gene transfer mediated by lipo- and polyplexes. *Mol. Ther.* **12,** 468–474.

Rouse, J. G., Yang, J., Barron, A. R., and Monteiro-Riviere, N. A. (2006). Fullerene-based amino acid nanoparticle interactions with human epidermal keratinocytes. *Toxicol. In Vitro.* **8,** 1313–1320.

Ryman-Rasmussen, J. P., Riviere, J. E., and Monteiro-Riviere, N. A. (2006). Penetration of intact skin by quantum dots with diverse physicochemical properties. *Toxicol. Sci.* **9,** 159–165.

Ryman-Rasmussen, J. P., Riviere, J. E., and Monteiro-Riviere, N. A. (2007a). Surface coatings determine cytotoxicity and irritation potential of quantum dot nanoparticles in epidermal keratinocytes. *J. Invest. Dermatol.* **127,** 143–153.

Ryman-Rasmussen, J. P., Riviere, J. E., and Monteiro-Riviere, N. A. (2007b). Variables influencing interactions of untargeted quantum dot nanoparticles with skin cells and identification of biochemical modulators. *Nano Lett.* **7,** 1344–1348.

Saif, Y. M., Saif, L. J., Hofacre, C. L., Hayhow, C., Swayne, D. E., and Dearth, R. N. (1990). A small round virus associated with enteritis in turkey poults. *Avian Dis.* **34,** 762–764.

Sayes, C. M., Fortner, J. D., Guo, W., Lyon, D., Boyd, A. M., Ausman, K. D., Tao, Y. J., Sitharaman, B., Wilson, L. J., Hughes, J. B., *et al.* (2004). The differential cytotoxicity of water-soluble fullerenes. *Nano Lett.* **4,** 1881–1887.

Schafer, D. A. (2002). Coupling actin dynamics and membrane dynamics during endocytosis. *Curr. Opin. Cell Biol.* **14,** 76–81.

Scott, G., Leopardi, S., Parker, L., Babiarz, L., Seiberg, M., and Han, R. (2003). The proteinase-activated receptor-2 mediates phagocytosis in a Rho-dependent manner in human keratinocytes. *J. Invest. Dermatol.* **121,** 529–541.

Seglen, P. O. (1983). Inhibitors of lysosomal function. *Methods Enzymol.* **96,** 737–764.

Seiberg, M., Paine, C., Sharlow, E., Andrade-Gordon, P., Costanzo, M., Eisinger, M., and Shapiro, S. S. (2000). Inhibition of melanosome transfer results in skin lightening. *J. Invest. Dermatol.* **115,** 162–167.

Sharlow, E. R., Paine, C. S., Babiarz, L., Eisinger, M., Shapiro, S., and Seiberg, M. (2000). The protease-activated receptor-2 upregulates keratinocyte phagocytosis. *J. Cell. Sci.* **113,** 3093–3101.

Sieczkarski, S. B., and Whittaker, G. R. (2002). Dissecting virus entry via endocytosis. *J. Gen. Virol.* **83,** 1535–1545.

Stuart, A. D., and Brown, T. D. (2006). Entry of feline calicivirus is dependent on clathrin-mediated endocytosis and acidification in endosomes. *J. Virol.* **80,** 7500–7509.

Swannie, H. C., and Kaye, S. B. (2002). Protein kinase C inhibitors. *Curr. Oncol. Rep.* **4,** 37–46.

Swanson, J. A., and Watts, C. (1995). Macropinocytosis. *Trends Cell Biol.* **11,** 424–428.

Tebar, F., Sorkina, T., Sorkin, A., Ericsson, M., and Kirchhausen, T. (1996). Eps15 is a component of clathrin-coated pits and vesicles and is located at the rim of coated pits. *J. Biol. Chem.* **271,** 28727–28730.

te Pas, M. F., Lombardi, P., Havekes, L. M., Boonstra, J., and Ponec, M. (1991). Regulation of low-density lipoprotein receptor expression during keratinocyte differentiation. *J. Invest. Dermatol.* **97,** 334–339.

Tjelle, T. E., Brech, A., Juvet, L. K., Griffiths, G., and Berg, T. (1996). Isolation and characterization of early endosomes, late endosomes and terminal lysosomes: their role in protein degradation. *J. Cell. Sci.* **109,** 2905–2914.

Tsuruoka, H., Khovidhunkit, W., Brown, B. E., Fluhr, J. W., Elias, P. M., and Feingold, K. R. (2002). Scavenger receptor class B type I is expressed in cultured keratinocytes and epidermis. Regulation in response to changes in cholesterol homeostasis and barrier requirements. *J. Biol. Chem.* **277,** 2916–2922.

von Hahn, T., Lindenbach, B. D., Boullier, A., Quehenberger, O., Paulson, M., Rice, C. M., and McKeating, J. A. (2006). Oxidized low-density lipoprotein inhibits hepatitis C virus cell entry in human hepatoma cells. *Hepatology* **43,** 932–942.

van Weert, A. W., Dunn, K. W., Gueze, H. J., Maxfield, F. R., and Stoorvogel, W. (1995). Transport from late endosomes to lysosomes, but not sorting of integral membrane proteins in endosomes, depends on the vacuolar proton pump. *J. Cell. Biol.* **130,** 21–34.

Wagner, M., Rajasekaran, A. K., Hanzel, D. K., Mayor, S., and Rodriguez-Boulan, E. (1994). Brefeldin A causes structural and functional alterations of the trans-Golgi network of MDCK cells. *J. Cell. Sci.* **107,** 933–943.

Wang, C. H., Wu, C. Y., and Lo, C. F. J. (1999). A new picorna-like virus, PnPV, isolated from ficus transparent wing moth, Perina nuda (Fabricius). *Invertebr. Pathol.* **74,** 62–68.

Wang, L. H., Rothberg, K. G., and Anderson, R. G. (1993). Mis-assembly of clathrin lattices on endosomes reveals a regulatory switch for coated pit formation. *J. Cell. Biol.* **123,** 1107–1117.

Wang, Y., Li, D., Fan, H., Tian, L., Zhong, Y., Zhang, Y., Yuan, L., Jin, C., Yin, C., and Ma, D. (2006). Cellular uptake of exogenous human PDCD5 protein. *J. Biol. Chem.* **281,** 24803–24817.

Whitman, S. C., Daugherty, A., and Post, S. R. (2000). Regulation of acetylated low density lipoprotein uptake in macrophages by pertussis toxin-sensitive G proteins. *J. Lipid Res.* **41,** 807–813.

Xia, T., Kovochich, M., Liong, M., Zink, J. I., and Nel, A. E. (2008). Cationic polystyrene nanosphere toxicity depends on cell-specific endocytic and mitochondrial injury pathways. *ACS Nano* **2,** 85–96.

Xing, Y., Chaudry, Q., Shen, C., Kong, K. Y., Zhau, H. E., Chung, L. W., Petros, J. A., O'Regan, R. M., Yezhelyev, M. V., Simons, J. W., *et al.* (2007). Bioconjugated quantum dots for multiplexed and quantitative immunohistochemistry. *Nat. Protoc.* **2,** 1152–1165.

Yamane, K., Kataoka, S., Le, N. A., Paidi, M., Howard, W. J., Hannah, J. S., and Howard, B. V. (1996). Binding affinity and particle size of LDL in subjects with moderate hypercholesterolemia: relationship with in vivo LDL metabolism. *J. Lipid Res.* **37,** 1646–1654.

Zhang, L. W., Yu, W. W., Colvin, V. L., and Monteiro-Riviere, N. A. (2008). Biological interactions of quantum dot nanoparticles in skin and in human epidermal keratinocytes. *Toxicol. Appl. Pharmacol.* **228,** 200–211.

Zhang, L. W., Zeng, L., Barron, A. R., and Monteiro-Riviere, N. A. (2007). Biological interactions of functionalized single-wall carbon nanotubes in human epidermal keratinocytes. *Int. J. Toxicol.* **26,** 103–113.

Zhang, Y., Kohler, N., and Zhang, M. (2002). Surface modification of superparamagnetic magnetite nanoparticles and their intracellular uptake. *Biomaterials* **23,** 1553–1561.